





Research Article

<https://doi.org/10.1631/jzus.B2300138>

Nrf2-mediated ferroptosis of spermatogenic cells involved in male reproductive toxicity induced by polystyrene nanoplastics in mice

Xufeng FU^{1,2*}, Hang HAN^{1*}, Hong YANG¹, Bo XU¹, Wenjie DAI¹, Ling LIU¹, Tiantian HE¹, Xing DU¹,
Xiuying PEI^{1,2}

¹Key Laboratory of Fertility Preservation and Maintenance of Ministry of Education, School of Basic Medical Sciences, Ningxia Medical University, Yinchuan 750004, China

²Key Laboratory of Reproduction and Genetics in Ningxia, Ningxia Medical University, Yinchuan 750004, China

Abstract: Microplastics (MPs) and nanoplastics (NPs) have become hazardous materials due to the massive amount of plastic waste and disposable masks, but their specific health effects remain uncertain. In this study, fluorescence-labeled polystyrene NPs (PS-NPs) were injected into the circulatory systems of mice to determine the distribution and potential toxic effects of NPs in vivo. Interestingly, whole-body imaging found that PS-NPs accumulated in the testes of mice. Therefore, the toxic effects of PS-NPs on the reproduction systems and the spermatocytes cell line of male mice, and their mechanisms, were investigated. After oral exposure to PS-NPs, their spermatogenesis was affected and the spermatogenic cells were damaged. The spermatocyte cell line GC-2 was exposed to PS-NPs and analyzed using RNA sequencing (RNA-seq) to determine the toxic mechanisms; a ferroptosis pathway was found after PS-NP exposure. The phenomena and indicators of ferroptosis were then determined and verified by ferroptosis inhibitor ferrostatin-1 (Fer-1), and it was also found that nuclear factor erythroid 2-related factor 2 (Nrf2) played an important role in spermatogenic cell ferroptosis induced by PS-NPs. Finally, it was confirmed in vivo that this mechanism of Nrf2 played a protective role in PS-NPs-induced male reproductive toxicity. This study demonstrated that PS-NPs induce male reproductive dysfunction in mice by causing spermatogenic cell ferroptosis dependent on Nrf2.

Key words: Polystyrene nanoplastics (PS-NPs); Reproductive toxicity; Ferroptosis; Nuclear factor erythroid 2-related factor 2 (Nrf2)

1 Introduction


Currently, plastics are widely used in various manufacturing industries, such as food packaging, children's toys, clothing materials, medical instruments, and building materials, and even in daily life, due to their low cost and convenient properties (Li YM et al., 2021). In 2018, more than 360 million tons of plastics were produced worldwide (Kedzierski et al., 2020). In the natural environment, bulk plastic waste can undergo fragmentation into smaller pieces (microplastics (MPs): <5 mm in diameter; nanoplastics (NPs): 1–100 nm

in diameter) that pose a threat to a diverse range of organisms (Wang LW et al., 2021). In addition, numerous studies have demonstrated that the many disposable masks consumed during the coronavirus disease-2019 (COVID-19) epidemic released MPs/NPs into the environment by natural weathering (Wang Z et al., 2021; Shukla et al., 2022). Previous studies have shown that smaller NPs are more likely to remain in organisms than larger ones, which may be related to the fact that NPs with smaller particles find it easier to enter and stay in cells and cause cytotoxicity (Rist et al., 2017; Fu et al., 2023). It is currently impossible to accurately assess the formation rate of NPs in the environment and the metabolic rate in vivo due to the limitations of technology; thus, NPs are regarded as a novel persistent environmental contaminant that poses significant risks to human health (Khan et al., 2022). In addition, NPs can be transferred to humans through the food chain, from marine plankton to fish or seafood (Wang LW et al., 2021; Yosri et al., 2021). On the other

✉ Xing DU, duxingok@126.com

Xiuying PEI, peixiuying@163.com

* The two authors contributed equally to this work

 Xufeng FU, <https://orcid.org/0000-0002-4101-1000>

Xing DU, <https://orcid.org/0000-0003-2683-4524>

Xiuying PEI, <https://orcid.org/0000-0002-4410-8588>

Received Feb. 28, 2023; Revision accepted July 29, 2023;
Crosschecked Mar. 13, 2024

© Zhejiang University Press 2024

hand, NPs can accumulate in plants, move to a higher trophic level, and eventually enter humans (Yin LS et al., 2021). To date, NPs have been found in drinking water (Oßmann et al., 2018), food (Kedzierski et al., 2020), air (Gasperi et al., 2018), teabags (Hernandez et al., 2019), take-out food containers (Du et al., 2020), and personal care products (Fendall and Sewell, 2009). Studies have also demonstrated the direct routes of NPs' exposure in the human body through the gastrointestinal system, respiratory tract inhalation, and skin penetration (Yee et al., 2021). Furthermore, after intake, NPs can enter the blood and lymphatic circulatory systems and distribute to various organs, including the brain, liver, heart, reproductive organs, and even the human placenta (Ragusa et al., 2021; Yin K et al., 2021).

Reproductive health is critical to human health and is the key to the quality of human offspring. Recently, infertility has been a major public health problem worldwide. It is estimated that nearly 12% of couples worldwide are infertile, of which 50% are caused by male infertility (Schulte et al., 2010; Zegers-Hochschild et al., 2017). From 1973 to 2011, the number of sperms decreased by 50%–60% globally (Levine et al., 2017) and, from 2001 to 2015, the proportion of sperms with normal morphology decreased from 31.8% to 10.8% in China (Huang et al., 2017). Oxidative stress constitutes a significant etiological factor in male infertility, which is essentially due to the imbalance of intracellular reactive oxygen species (ROS) and antioxidation in spermatids (Bisht et al., 2017). Approximately 80% of male infertility cases are attributed to high levels of ROS in semen, leading to what is known as male oxidative stress infertility (MOSI). As a result, it would be useful to understand the underlying toxicological mechanisms by which NPs cause adverse effects on male reproduction.

In the present study, the adverse effects of 50- and 90-nm polystyrene nanoparticles (PS-NPs) on male reproduction as well as underlying mechanisms were assessed in mice.

2 Results

2.1 Induction of male reproductive toxicity in mice by PS-NPs

To determine the adverse effects of NPs, two PS-NPs (diameter sizes of 50 and 90 nm, respectively)

were chosen to compare the toxicity *in vivo* and *in vitro*. First, the characteristics of two types of PS-NPs, including size and shape, were determined using transmission electron microscopy (TEM), and the particles presented a near-spherical shape and adequate particle diameter size, consistent with the commercial test report (Fig. 1a). Mice were infused with fluorescence-labeled PS-NPs (50 nm) via intravenous tail injection for two days to investigate the distribution and accumulation of NPs *in vivo*. Interestingly, the result revealed that PS-NPs were distributed and accumulated in the testes of mice (Fig. 1b). To further determine the distribution and accumulation of PS-NPs in tissues and organs, the mice were euthanized, and their organs were harvested. The fluorescence imaging assay revealed that the fluorescence-labeled PS-NPs were accumulated in the brain, lung, testis, heart, kidney, epididymis, and liver rather than in the spleen (Fig. 1c). This result suggested that PS-NPs entering the blood circulatory system may be more likely to accumulate in these organs or tissues. To determine the specific male reproductive toxicity of PS-NPs at the nano-scale, pristine PS-NPs of 50 and 90 nm were exposed to male mice for 30, 45, and 60 d. After 50 nm PS-NP exposure for 30 d, the testicular morphology was significantly more decreased than in the control (Fig. 1d), the sperm morphology and semen quality were detected, and the results are displayed in Fig. S1. The results demonstrated that sperm morphology was affected (Fig. S1a), testosterone level was decreased (Fig. S1b), the sperm viability was decreased (Fig. S1c), and the sperm abnormality rate was increased (Fig. S1d) after 50 nm PS-NP exposure for 30 d. After 90 nm PS-NP exposure for 30 d, the result revealed that the sperm morphology was affected (Fig. S1e), testosterone level was decreased (Fig. S1f), the sperm concentration was decreased (Fig. S1g), the sperm viability was decreased (Fig. S1h), and the sperm abnormality rate was increased (Fig. S1i). Fig. S2 illustrates the testicular morphology (Fig. S2a), sperm concentration (Fig. S2b), viability (Fig. S2c), and abnormality rate (Fig. S2d) after 50 nm PS-NP exposure for 45 d. Fig. S3 shows the testicular morphology (Fig. S3a), the sperm concentration (Fig. S3b), viability (Fig. S3c), and abnormality rate (Fig. S3d) after 50 nm PS-NP exposure for 60 d. Additionally, body weight was evaluated in 50 nm PS-NP exposure for 60 d at intervals of seven days, and the result demonstrated insignificant differences between the control and

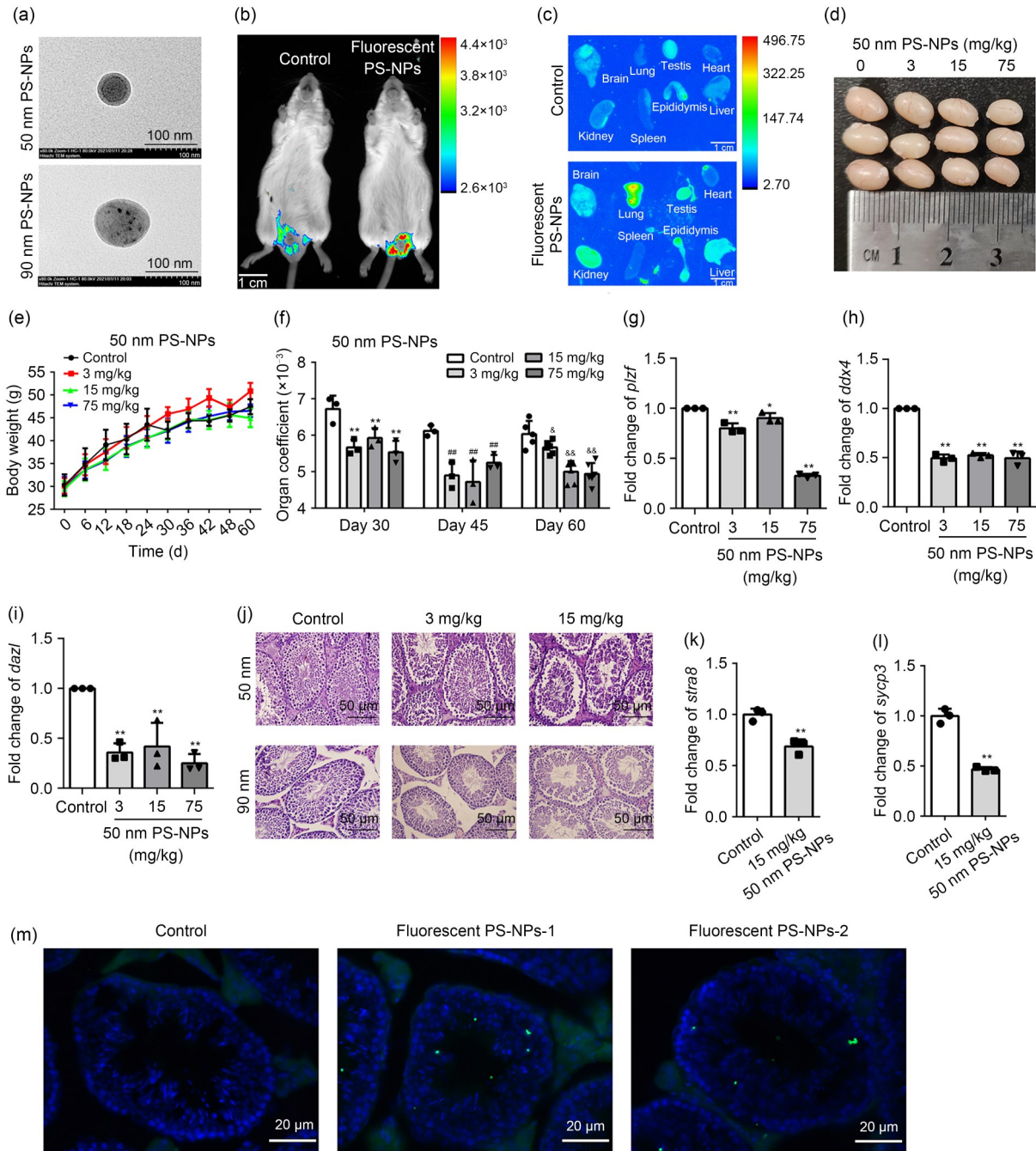


Fig. 1 Effects of PS-NPs on male reproductive toxicity by damaging spermatogenesis. (a) The characterization of 50 nm and 90 nm PS-NPs. (b) The whole-animal fluorescence imaging after fluorescence-labeled PS-NP intravenous tail injection. (c) The fluorescence imaging of fluorescence-labeled PS-NPs accumulated in various organs. (d) The testicular morphology of mice after 50 nm PS-NP exposure for 30 d. (e) The body weight of mice after 50 nm PS-NP exposure for 60 d. (f) The organ coefficients of testes after 50 nm PS-NP exposure for 30, 45, and 60 d. (g–i) The gene expression of *plzf* (g), *ddx4* (h), and *dazl* (i) in testis after 50 nm PS-NP exposure for 30 d. (j) The testicular histology of 50 and 90 nm PS-NP exposure for 30 d. (k, l) The expression of meiosis genes *stra8* (k) and *sycp3* (l) in testicular tissue after 50 nm PS-NP exposure for 30 d. (m) The fluorescent PS-NPs emerged in seminiferous tubules. Data are expressed as mean±standard deviation (SD), $n=3$. * $P<0.05$, ** $P<0.01$, compared with the control in the 30-d exposed group; ## $P<0.01$, compared with the control in the 45-d exposed group; & $P<0.05$, && $P<0.01$, compared with the control in the 60-d exposed group. PS-NPs: polystyrene nanoparticles; *plzf*: promyelocytic leukemia zinc finger; *ddx4*: (Asp-Glu-Ala-Asp, DEAD)-box helicase 4; *dazl*: deleted in azoospermia (DAZ)-like; *stra8*: stimulated by retinoic acid 8; *sycp3*: synaptonemal complex protein 3.

exposed groups (Fig. 1e). The organ coefficient of testes was determined accordingly, and the result revealed that the organ coefficients decreased after 30, 45, and 60 d of exposure (Fig. 1f). These results suggested that PS-NPs can induce male reproductive toxicity in mice.

2.2 Effect of PS-NPs on spermatogenesis by damaging spermatocyte

The expression of spermatogenesis-related genes was detected to determine the effect in the testis caused by PS-NPs. The results demonstrated that the expression levels of promyelocytic leukemia zinc finger (*plzf*) (Fig. 1g), (Asp-Glu-Ala-Asp, DEAD)-box helicase 4 (*ddx4*) (Fig. 1h), and deleted in azoospermia (DAZ)-like (*dazl*) (Fig. 1i) were decreased after 50 nm PS-NP exposure for 30 and 60 d (Figs. S3e–S3g), suggesting that PS-NPs could affect spermatogenesis. Then, the testicular histology was evaluated, and the result revealed that the layers of spermatogenic cells were lost in the seminiferous tubules after 50 and 90 nm PS-NP exposure for 30 d (Fig. 1j), 45 d (Fig. S2e), and 60 d (Fig. S3h). These results implied that spermatogenic cells might be one of the cells damaged by PS-NPs. The expression of key genes stimulated by retinoic acid 8 (*stra8*) and synaptonemal complex protein 3 (*sycp3*) in spermatocyte meiosis was detected to confirm the hypothesis. The results demonstrated that the expression of *stra8* (Fig. 1k) and *sycp3* (Fig. 1l) decreased after 50 nm PS-NP exposure for 30 d. In addition, the fluorescence-labeled PS-NPs were found in the seminiferous tubule after two days by tail vein injection (Fig. 1m). These results suggested that PS-NPs could cross the blood–testis barrier and damage the function of spermatogenic cells in seminiferous tubules.

2.3 Effect of PS-NPs on the viability of GC-2 cells through ferroptosis

To explore the mechanisms by which PS-NPs affect spermatogenic cells, the spermatocyte cell line GC-2 was employed to evaluate the cytotoxicity of PS-NPs in vitro. To investigate the cytotoxicity of PS-NPs to GC-2 cells, the fluorescence-labeled PS-NPs (50 nm) were used to expose GC-2 cells for 24 h. The result demonstrated that PS-NPs were internalized in the cytoplasm of GC-2 cells (Fig. 2a). Then, the cytotoxicity of PS-NPs in GC-2 cells for 24 h was determined by the cell counting kit-8 (CCK8) assay. The results demonstrated that 50 nm PS-NPs significantly affected

cell viability at 25 µg/mL or higher concentrations (Fig. 2b), and 90 nm PS-NPs required a higher concentration at 75 µg/mL to reduce cell viability (Fig. 2c). These results might suggest an inverse correlation between the diameter size of PS-NPs and their cytotoxicity. RNA sequencing (RNA-seq) was performed to investigate the detailed cytotoxicity mechanisms of PS-NPs' impacts on GC-2 cells. The result demonstrated that 240 genes were upregulated and 210 genes were downregulated after 50 nm PS-NP exposure, and 458 were upregulated and 223 were downregulated after 90 nm PS-NP exposure, compared to the control (Fig. 2d). After enrichment analysis, the results demonstrated that parts of the differential genes were enriched in ferroptosis and the redox reaction signaling pathway in both the 50 nm (Fig. 2e) and 90 nm (Fig. 2f) PS-NP-treated groups. It is suggested that the effect of PS-NP exposure on cell viability may be caused by ferroptosis. Ferroptosis is a new programmed cell death (PCD) type proposed recently, and it is independent of apoptosis, necrosis, and autophagy (Dixon et al., 2012). The failure of the cell membrane lipid repairing enzyme glutathione peroxidase 4 (GPX4) leads to reductive glutathione depletion and an increase in free Fe²⁺, which can oxidize lipids via the Fenton reaction, resulting in the production of a large amount of lipid ROS, which destroys intracellular redox homeostasis and eventually causes cell death (Dixon et al., 2012; Hassannia et al., 2019). To confirm this hypothesis, the inhibitors of apoptosis (Z-VAD-FMK), necrosis (necrostatin-1), and ferroptosis (ferrostatin-1 (Fer-1)) were employed to restore the PS-NP-affected viability. The result revealed that only the inhibitor of ferroptosis Fer-1 could significantly rescue the GC-2 viability affected by PS-NPs (Fig. 2g). These results implied that PS-NPs affect GC-2 viability through iron metabolism and redox destruction. Therefore, nuclear factor erythroid 2-related factor 2 (Nrf2) and GPX4, the key proteins of redox and ferroptosis, were detected by western blotting. The results demonstrated that the expression of Nrf2 and GPX4 significantly changed after 50 and 90 nm PS-NP exposure at 12.5 µg/mL (Fig. 2h) and 25 µg/mL (Fig. 2i), respectively. Additionally, the malonaldehyde (MDA) results showed that lipid peroxidation level was affected by 12.5 µg/mL 50 nm PS-NPs (Fig. 2j), 25 µg/mL 90 nm PS-NPs (Fig. 2k), or higher concentrations. Consequently, acquiring these treated concentrations provided a reference basis for

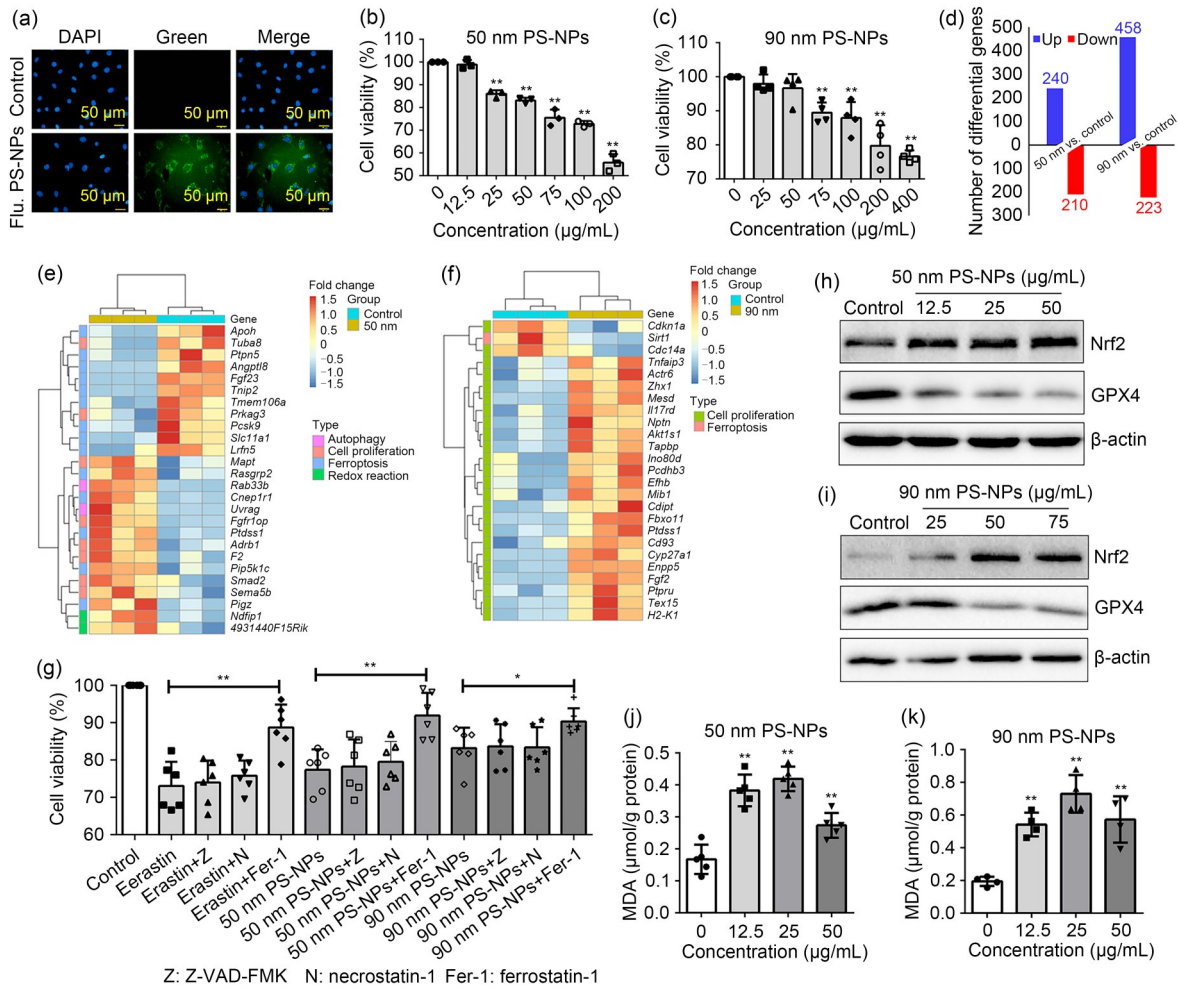


Fig. 2 Effects of PS-NPs on the viability of GC-2 cells through ferroptosis. (a) The 50 nm fluorescent (Flu.) PS-NPs were internalized in the cytoplasm of GC-2 cells. (b, c) The viabilities of GC-2 cells after 50 nm (b) and 90 nm (c) PS-NPs at a series of concentrations. (d) The number of differential genes after 50 and 90 nm PS-NP exposure compared with control. (e, f) The differential genes affecting cell viabilities after 50 nm (e) and 90 nm (f) PS-NP exposure are enriched in the ferroptosis pathway. (g) GC-2 viability was rescued by an inhibitor of ferroptosis rather than inhibitors of apoptosis and necrosis. (h, i) Nrf2 and GPX4 expression in GC-2 cells after 50 nm (h) and 90 nm (i) PS-NP exposure. (j, k) MDA levels in GC-2 cells after 50 nm (j) and 90 nm (k) PS-NP exposure. Data are expressed as mean \pm standard deviation (SD), $n=4$ or 6 . * $P<0.05$, ** $P<0.01$, compared with the control group. PS-NPs: polystyrene nanoparticles; DAPI: 4',6-diamidino-2-phenylindole; Nrf2: nuclear factor erythroid 2-related factor 2; GPX4: glutathione peroxidase 4; MDA: malonaldehyde.

subsequent experiments. Additionally, the expression of proteins associated with ferroptosis, such as Nrf2 and GPX4, and redox levels, such as MDA, glutathione (GSH), and superoxide dismutase (SOD), were detected in the testes (Fig. S4). These results suggested that PS-NPs triggered ferroptosis in GC-2 cells.

2.4 Effect of PS-NPs on the appearance of ferroptosis characteristics in GC-2 cells

To observe the ferroptosis after PS-NP exposure, the characteristics of ferroptosis, including mitochondrial structure and function, were determined in GC-2

cells, which were exposed to 50 and 90 nm PS-NPs at 12.5 and 25 $\mu\text{g/mL}$ for 24 h, respectively. Subsequently, the morphology of mitochondria was detected using TEM. Compared to the control group, PS-NPs-exposed GC-2 cells displayed morphological features associated with ferroptosis, such as mitochondrial shrinkage or matrix condensation, cristae decrease or disappearance, and increased outer membrane density (Fig. 3a). Then, the result of cellular free divalent iron demonstrated an apparent increase in the PS-NPs-exposed group compared to the control group (Fig. 3b). Meanwhile, the level of lipid peroxidation was detected by

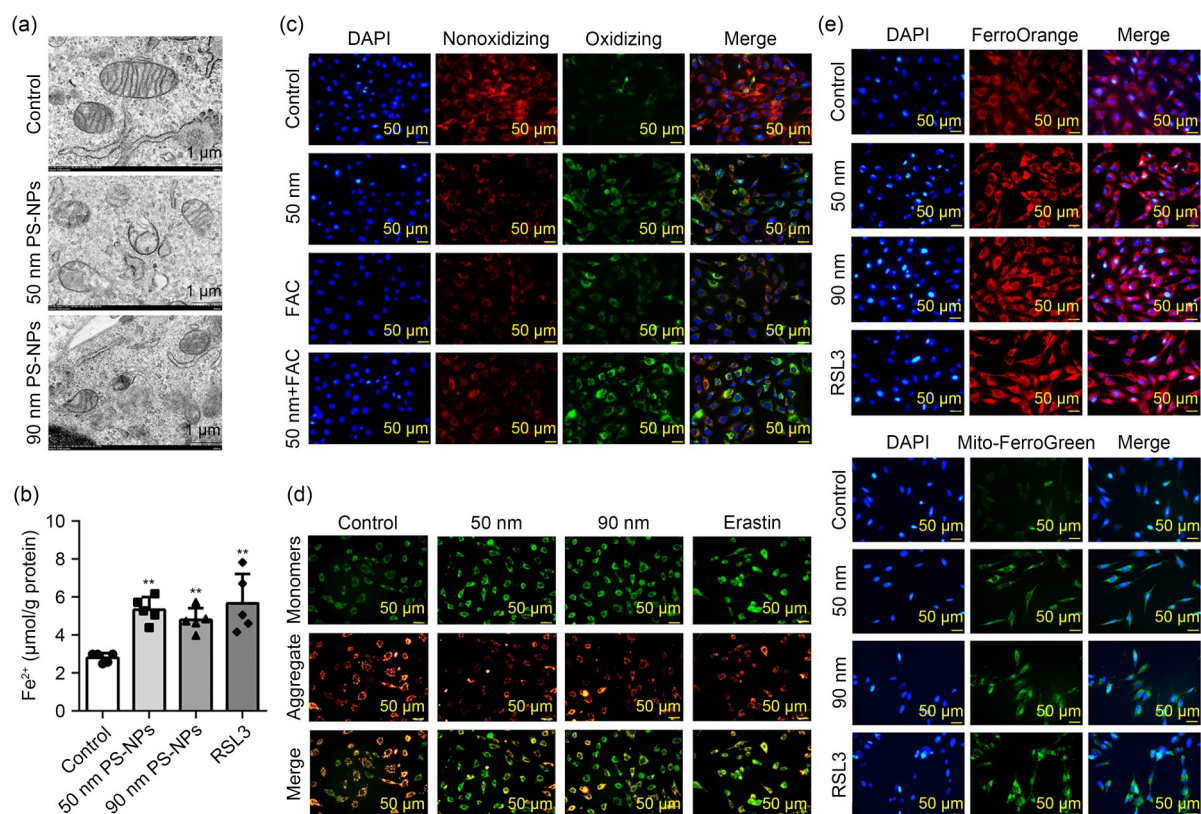


Fig. 3 Effect of PS-NPs on the appearance of ferroptosis characteristics in GC-2 cells. (a) The morphology of mitochondria under transmission electron microscopy in GC-2 cells after PS-NP exposure. (b) The level of cellular free divalent iron in GC-2 cells after PS-NP exposure; RSL3 is an inhibitor of GPX4 and serves as a positive control. (c) The level of lipid peroxidation in GC-2 cells was detected by C11 BODIPY 581/591 after PS-NP exposure; FAC is a ferric ion provider and serves as a positive control. (d) The change of mitochondrial membrane potential (MMP) in GC-2 cells was tested by JC-1 fluorescent dye after PS-NP exposure. (e) The levels of labile ferrous ion in the cytoplasm and mitochondria of GC-2 cells were verified by FerroOrange and Mito-FerroGreen fluorescence probe detection after PS-NP exposure, respectively. RSL3 (inhibitor of GPX4) serves as a positive control. Data are expressed as mean±standard deviation (SD), $n=5$. ** $P<0.01$, compared with the control group. PS-NPs: polystyrene nanoparticles; GPX4: glutathione peroxidase 4; FAC: ferrous ammonium citrate; DAPI: 4',6-diamidino-2-phenylindole.

a lipid peroxidation fluorescence sensor (C11 BODIPY 581/591), and the result showed that 50 nm PS-NPs accelerated the production of lipid ROS. The combined exposure of 50 nm PS-NPs and ferric ion provider ferrous ammonium citrate (FAC) resulted in a higher level of lipid ROS than PS-NP exposure alone, indicating that PS-NPs induced an increase in the oxidized form and a decrease in the reduced form of lipid molecules in GC-2 cells after PS-NP exposure (Fig. 3c). Furthermore, the mitochondrial membrane potential (MMP) was tested with JC-1 fluorescent dye. The result demonstrated a transition from red to green fluorescence after treatment with PS-NPs, indicating decreased PS-NPs-induced MMP in GC-2 cells (Fig. 3d). The levels of labile ferrous ion in cytoplasm and mitochondria were confirmed using FerroOrange

and Mito-FerroGreen fluorescence probe detection, respectively. The results revealed that the levels of labile ferrous ion in cytoplasm and mitochondria were higher in PS-NPs-exposed groups than in the control group (Fig. 3e). RSL3 (inhibitor of GPX4), as a positive control, demonstrated a similar result with PS-NP exposure. These results suggested that ferroptosis appeared in GC-2 cells after exposure to 50 and 90 nm PS-NPs.

2.5 Effect of ferroptosis inhibitor ferrostatin-1 on PS-NPs-induced ferroptosis in GC-2 cells

To further investigate whether PS-NPs induce ferroptosis in GC-2 cells, the cells were co-cultured with ferroptosis inhibitor Fer-1 and PS-NPs. Ferroptosis events, including intracellular free divalent iron, MDA,

GSH, and protein expression in iron metabolism and antioxidant response, were then detected, including transferrin receptor (TFR), transferrin (TF), divalent metal transporter 1 (DMT1), ferroportin 1 (FPN1), GPX4, hemeoxygenase-1 (HO-1), and Nrf2. The findings demonstrated that Fer-1 could alleviate 50 and 90 nm PS-NPs-induced increased intracellular free divalent iron levels (Fig. 4a), high MDA levels (Fig. 4b), and low GSH levels (Fig. 4c). Moreover, the results of protein expression in iron metabolism and antioxidant response indicated that PS-NPs induced

proteins' expression changes in TFR (Figs. 4d and 4e), TF (Figs. 4d and 4f), DMT1 (Figs. 4d and 4g), FPN1 (Figs. 4d and 4h), GPX4 (Figs. 4d and 4i), HO-1 (Figs. 4d and 4j), and Nrf2 (Figs. 4d and 4k). Therefore, these results demonstrated that PS-NPs induced ferroptosis by increasing the expression of iron ion uptake and storage-related proteins (TFR, TF, and DMT1); meanwhile, PS-NPs decreased the expression of iron ion release protein (FPN1) and led to intracellular labile iron pool (LIP) accumulation and oxidant-antioxidant homeostasis destruction, thereby resulting in ferroptosis.

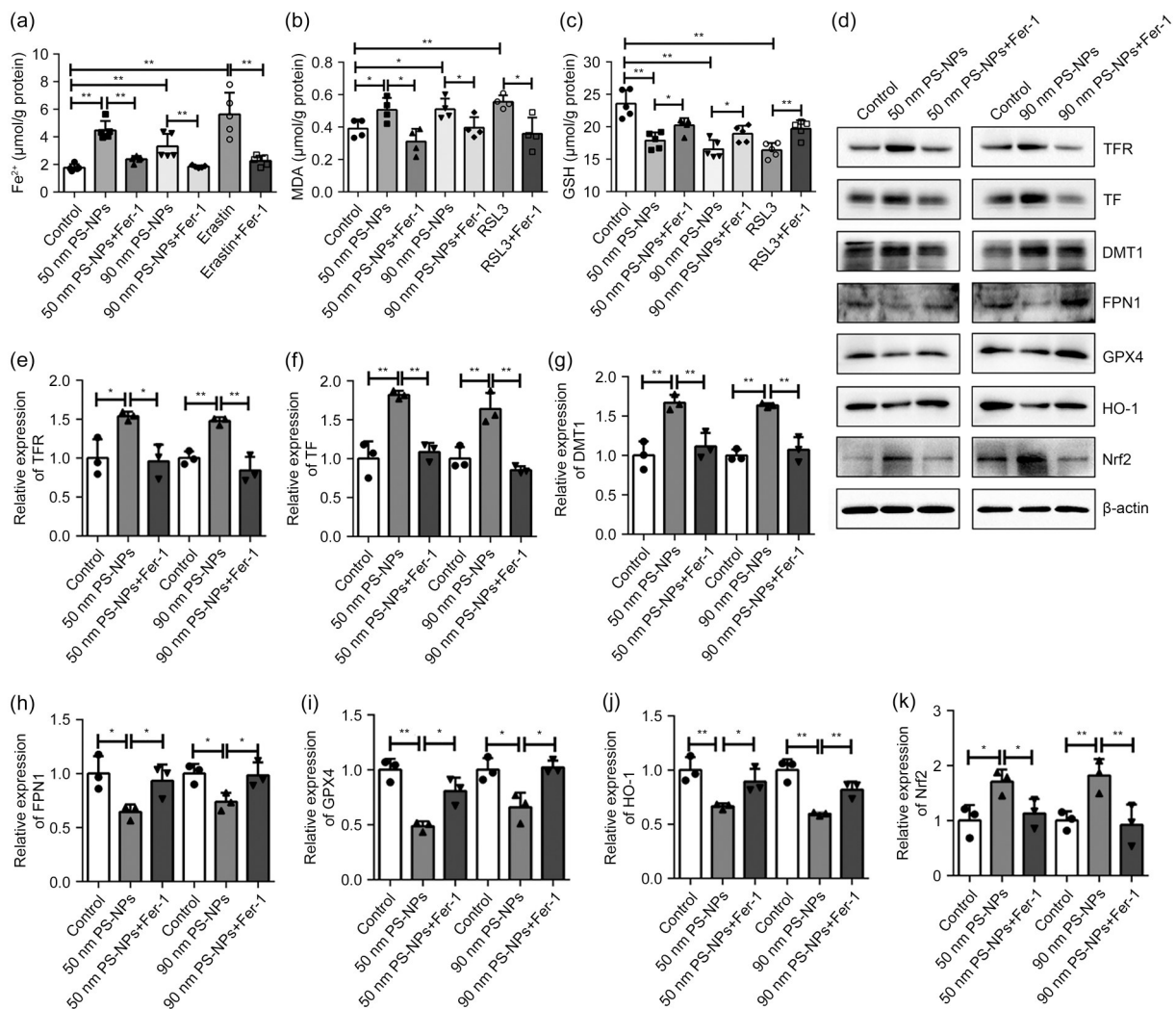


Fig. 4 Effect of ferroptosis inhibitor Fer-1 on PS-NPs-induced ferroptosis in GC-2 cells. (a–c) The high level of cellular free divalent iron (a), high level of MDA (b), and low level of GSH (c) in PS-NPs-exposed GC-2 cells were reversed by Fer-1. (d) The related protein expression levels involved in iron metabolism and antioxidant response after PS-NP exposure in GC-2 cells were reversed by Fer-1. (e–k) The expression of TFR (e), TF (f), DMT1 (g), FPN1 (h), GPX4 (i), HO-1 (j), and Nrf2 (k). Data are expressed as mean±standard deviation (SD), *n*=3, 4, or 5. * *P*<0.05, ** *P*<0.01, compared with the control group. Fer-1: ferrostatin-1; PS-NPs: polystyrene nanoparticles; MDA: malonaldehyde; GSH: glutathione; TFR: transferrin receptor; TF: transferrin; DMT1: divalent metal transporter 1; FPN1: ferroportin 1; GPX4: glutathione peroxidase 4; HO-1: hemeoxygenase-1; Nrf2: nuclear factor erythroid 2-related factor 2.

2.6 Effect of Nrf2 on the PS-NPs-induced ferroptosis in GC-2 cells

As illustrated in Figs. 2, 4, and S4, the expression of Nrf2 was increased after PS-NP exposure *in vivo* and *in vitro*. Furthermore, recent studies have demonstrated that Nrf2 plays a critical role in ferroptosis through transferring from cytoplasm to the nucleus, initiating gene expression of an antioxidant response (Sun et al., 2016; Dodson et al., 2019). The expression levels of Nrf2, Kelch-like ECH-associated protein 1 (Keap1, a moderator of Nrf2 proteasomal degradation), and GPX4 were detected to learn more about how Nrf2 regulates ferroptosis in PS-NPs-induced GC-2 cells. The results demonstrated that PS-NPs decreased the expression of GPX4 and Keap1, whereas they increased the expression of Nrf2 (Figs. 5a and S5a–S5c). Subsequently, the expression of Nrf2 in both the cytoplasm and the nucleus was detected, and the result indicated that Nrf2 was increased in the nucleus after PS-NP exposure, suggesting that PS-NPs may accelerate the dissociation of the interaction between Nrf2 and Keap1 and transfer from the cytoplasm into the nucleus (Figs. 5b, S5d, and S5e). To further confirm the hypothesis, the level of interaction between Nrf2 and Keap1 after PS-NP treatment was evaluated by co-immunoprecipitation with Keap1 antibody, and the result demonstrated that Nrf2 was decreased after PS-NP treatment (Fig. 5c), suggesting that PS-NPs could accelerate Nrf2 transferring into the nucleus and regulating the gene expression of an antioxidant response. Therefore, Nrf2 is considered a key regulator in PS-NPs and PS-NPs-induced ferroptosis. Then, the iron metabolism and antioxidant response tests were performed by interfering with the function and expression of Nrf2. The result revealed that Nrf2 inhibitor ML385 accelerated the expression of TFR and DMT1 while weakening the expression of FPN1, GPX4, and HO-1, which were compared with PS-NPs-treated GC-2 cells and the control (Figs. 5d and S5f–S5j). Moreover, the levels of cellular free divalent iron (Fig. 5e) and MDA (Fig. 5f) were higher while GSH (Fig. 5g) was lower in PS-NPs+ML385 groups than in only PS-NPs-treated groups. These results suggested that Nrf2 plays a protective role in PS-NPs-induced ferroptosis through its antioxidant response. Furthermore, the small interfering RNA (siRNA) sequences of Nrf2 were synthesized, and an optimized siRNA of No. 2 (Si-2) sequence was employed in subsequent studies (Fig. 5h). As expected,

the expression of FPN1, GPX4, and HO-1 was lower in Nrf2-interfering combined PS-NP treatment groups than in only PS-NPs-treated groups (Figs. 5i and S5k–S5n). These results suggested that PS-NPs accelerated ferroptosis when the function of Nrf2 was blocked, indicating that Nrf2 plays a protective role in PS-NPs-induced ferroptosis.

2.7 Effect of PS-NPs on male reproductive toxicity through Nrf2 regulating ferroptosis *in vivo*

To verify the hypothesis that PS-NPs induced male reproductive toxicity through Nrf2 regulating ferroptosis, the ferroptosis inhibitor Fer-1 and Nrf2 inhibitor ML385 were used in PS-NPs-exposed mice (Fig. 6a). After 30 d, the body weights of mice and male reproductive indicators in four groups (control, PS-NPs, PS-NPs+Fer-1, and PS-NPs+ML385) were evaluated. The results demonstrated that body weight was not influenced (Fig. 6b), while the reproductive indicators of the four groups were impacted. Figs. 6c and 6d show that PS-NPs decreased testicular morphology and organ coefficient, while Fer-1 rescued and ML385 aggravated the PS-NPs-influenced phenotype compared to the PS-NPs group. Analogously, the sperm concentration and abnormality rate were influenced by PS-NPs, while these effects were also rescued by Fer-1 and aggravated by ML385, compared to the PS-NPs group (Figs. 6e, 6g, and S6a). However, sperm viability seemed to have no changes due to Fer-1 or ML385 treatment in the PS-NP exposure group (Fig. 6f). The results of testicular histology demonstrated that a layer of cells in the seminiferous tubules was lost in the PS-NPs-exposed group, while this pathology was rescued by Fer-1 and seemingly aggravated by ML385 (Fig. 6h). From the immunohistochemistry results, GPX4 and FPN1 expression was decreased by PS-NPs, while Fer-1 rescued the decrease of PS-NPs-induced expression, and the expression of GPX4 or FPN1 was not changed by ML385 (Fig. 6h). Additionally, the expression of iron metabolism and antioxidant regulation-related proteins in the testes was detected, and the result showed that PS-NPs increased the expression of TFR, DMT1, and Nrf2, while Fer-1 decreased and ML385 aggravated PS-NPs-induced expression; PS-NPs decreased the expression of FPN1, GPX4, and HO-1, while Fer-1 increased and ML385 aggravated PS-NPs-induced expression. Although there was an insignificant difference

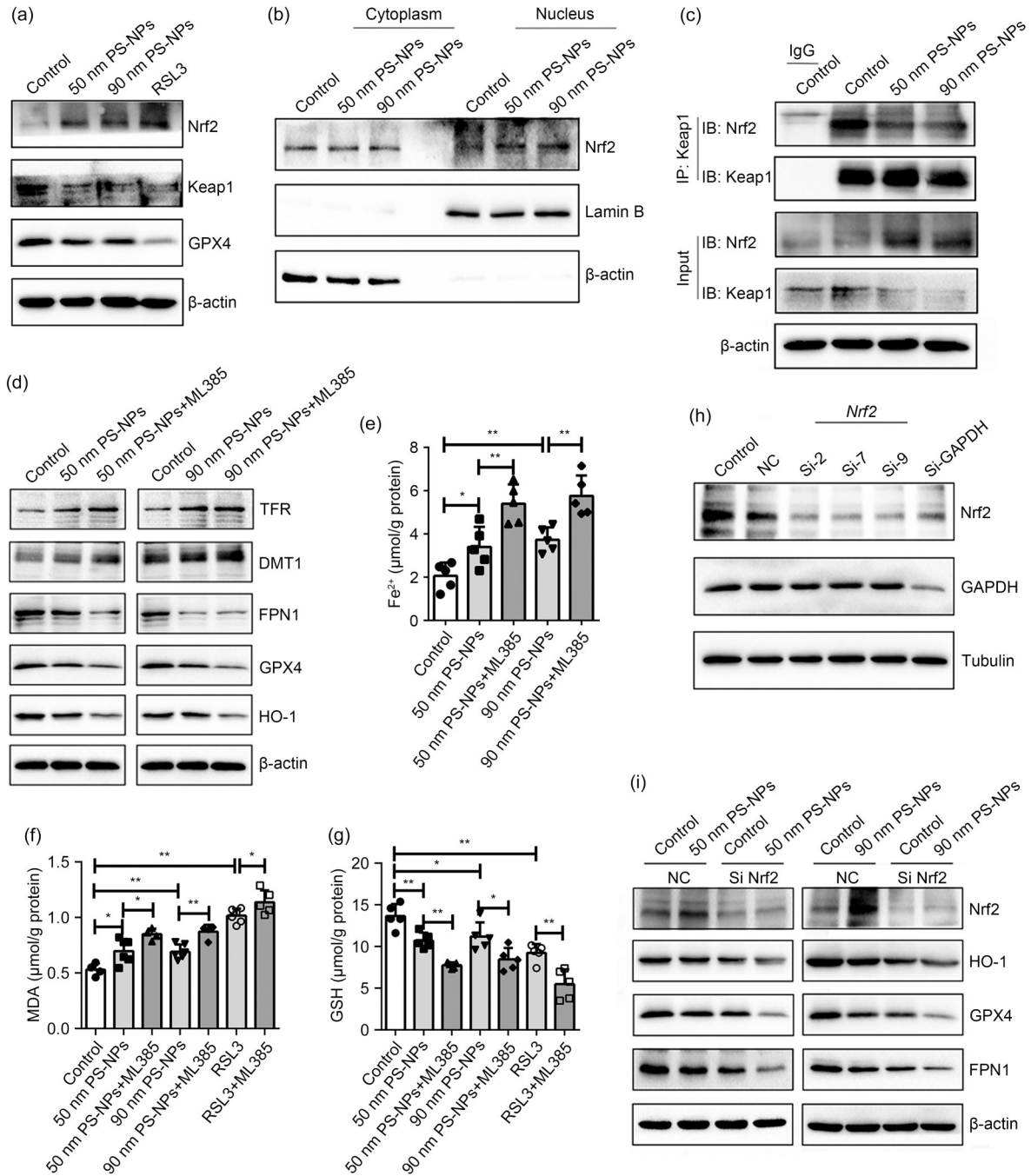


Fig. 5 Effect of Nrf2 on the PS-NPs-induced ferroptosis in GC-2 cells. (a) The expression of Nrf2, Keap1, and GPX4 after 50 and 90 nm PS-NP exposure. (b) Nrf2 expression in cytoplasm and nucleus after 50 and 90 nm PS-NP exposure. (c) Co-immunoprecipitation analysis of interaction between Keap1 and Nrf2, deposited by Keap1 antibody. (d) The expression of TFR, DMT1, FPN1, GPX4, and HO-1 after 50 and 90 nm PS-NP exposure, as well as Nrf2 inhibitor (ML385) addition. (e) Effect of PS-NPs on cellular free divalent iron after inhibiting Nrf2 by ML385. (f, g) MDA (f) and GSH (g) levels in GC-2 cells after PS-NP and ML385 co-treatment. (h) The optimized RNA interfering sequence of Nrf2 was screened by western blotting. (i) Expression of HO-1, GPX4, and FPN1 after PS-NP exposure as well as Nrf2 silencing. Data are expressed as mean±standard deviation (SD), $n=5$. * $P<0.05$, ** $P<0.01$, compared with the control group. Nrf2: nuclear factor erythroid 2-related factor 2; PS-NPs: polystyrene nanoparticles; IP: immunoprecipitation; Keap1: Kelch-like ECH-associated protein 1; GPX4: glutathione peroxidase 4; TFR: transferrin receptor; DMT1: divalent metal transporter 1; FPN1: ferroportin 1; HO-1: hemoxygenase-1; GAPDH: glyceraldehyde-3-phosphate dehydrogenase; NC: negative control; MDA malonaldehyde; GSH: glutathione; IgG: immunoglobulin G; Si-2: small interfering RNA of No. 2.

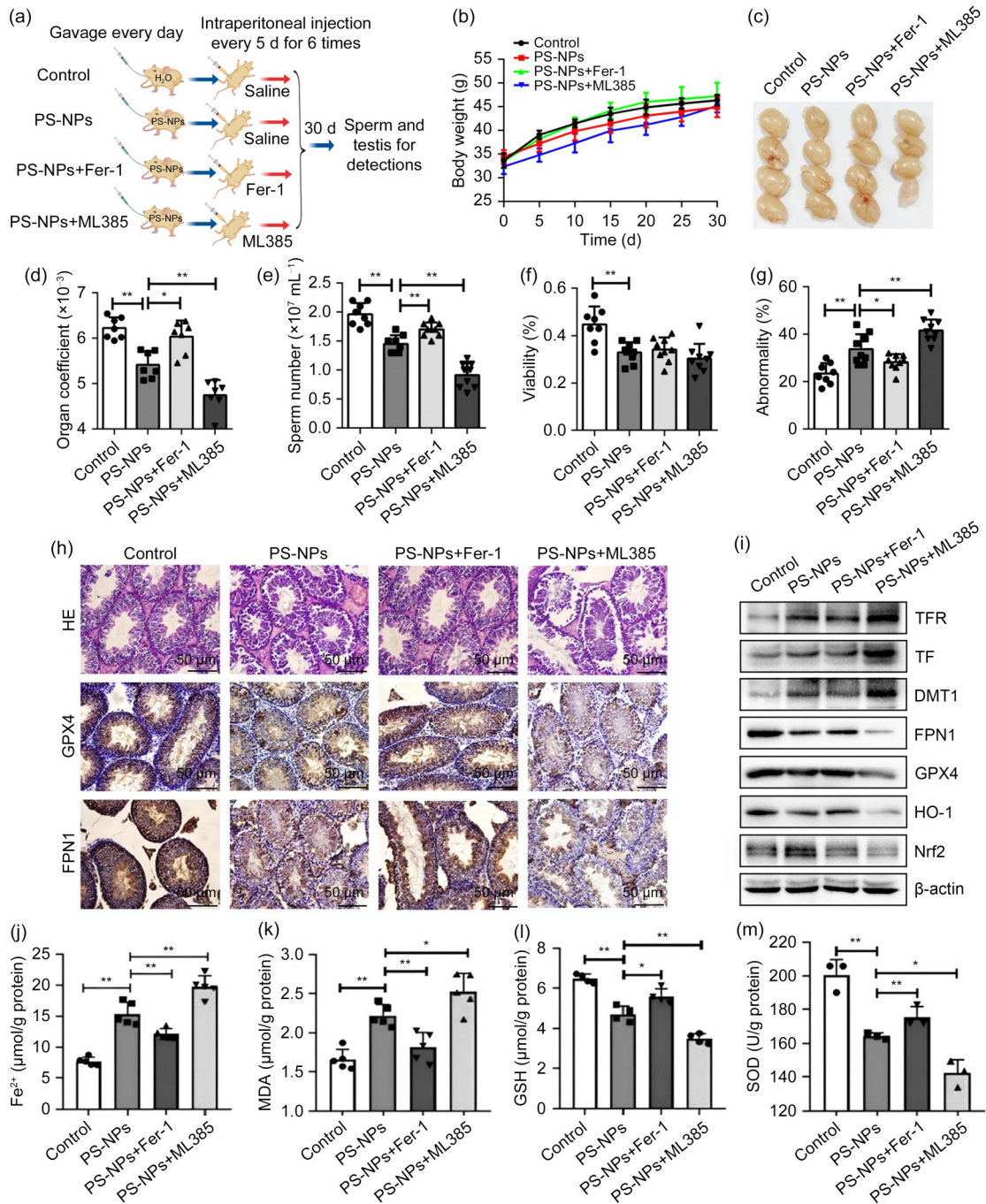


Fig. 6 Effect of PS-NPs on male reproductive toxicity through Nrf2 regulating ferroptosis in vivo. (a) The schematic drawing for verification that the male reproductive toxicity caused by PS-NPs-mediated Nrf2 regulates ferroptosis in vivo. (b) The body weights of Fer-1 (ferroptosis inhibitor)- and ML385 (Nrf2 inhibitor)-treated mice in PS-NP exposure period. (c–g) The testicular morphology (c), organ coefficient (d), sperm number (e), viability (f), and abnormality (g) of PS-NPs-exposed and Fer-1- and ML385-treated mice. (h) The testicular histology and immunohistochemistry of GPX4 and FPN1 expression in PS-NPs-exposed and Fer-1- and ML385-treated mice. (i) The expression of iron metabolism and antioxidant regulation-related proteins in the testes of PS-NPs-exposed and Fer-1- and ML385-treated mice. The levels of ferrous ion (j), MDA (k), GSH (l), and SOD (m) in the testes of PS-NPs-exposed and Fer-1- and ML385-treated mice. Data are expressed as mean \pm standard deviation (SD), $n=3, 4, 5, 6, 7,$ or 8 . * $P<0.05$, ** $P<0.01$, compared with the control group. PS-NPs: polystyrene nanoparticles; Nrf2: nuclear factor erythroid 2-related factor 2; Fer-1: ferrostatin-1; GPX4: glutathione peroxidase 4; FPN1: ferroportin 1; MDA: malonaldehyde; GSH: glutathione; SOD: superoxide dismutase; HE: hematoxylin-eosin; TFR: transferrin receptor; TF: transferrin; DMT1: divalent metal transporter 1; HO-1: hemeoxygenase-1.

in TF expression between the PS-NPs+Fer-1 group and the PS-NPs group, the PS-NPs+ML385 group revealed a significantly aggravated trend in PS-NPs-induced TF expression (Figs. 6i and S6b–S6h). Therefore, these protein expression *in vivo* showed similar trends to those *in vitro*. To further determine the effects of Fer-1 and ML385 on ferroptosis through iron metabolism and antioxidant regulation caused by PS-NPs, the levels of ferrous ion (Fig. 6j), MDA (Fig. 6k), GSH (Fig. 6l), and SOD (Fig. 6m) were tested, and the results showed that PS-NPs influenced ferrous ion level and antioxidant effect, while Fer-1 rescued and ML385 aggravated PS-NPs-induced influences. These results further suggested that PS-NPs cause male reproductive toxicity through ferroptosis of spermatogenic cells in mice, and Nrf2 plays a protective role in this process.

3 Discussion

Recently, increasing studies have reported the adverse effects and physiological toxicity of NPs to freshwater and marine organisms. Nonetheless, research into the biological effects of NPs on humans or other mammalian species is still lacking. Various toxicology studies have also demonstrated that NPs affect almost all organs and cells *in vivo* and *in vitro* (Yong et al., 2020; Yee et al., 2021). A recent study demonstrated that NPs have an endocrine disruptor effect and cause male reproductive toxicity (Amereh et al., 2020). However, it is unclear whether NPs can pass through the blood–testis barrier and affect spermatogenesis. To explore the bio-distribution and accumulation of NPs, we used 50 nm fluorescence-labeled PS-NPs by injecting them into the tail veins of mice for two days, and the results revealed that the high-intensity fluorescence signal was accumulated in the position of the testicles *in vivo*, and suggested that the fluorescence-labeled PS-NPs were accumulated in the brain, lung, heart, kidney, liver, epididymis, and testis. Consistent with our result, it has previously been reported that fluorescence-labeled PS-NPs were detected in the testis, brain, kidney, lung, and liver, and these results presented a high-intensity fluorescence signal in testicular tissue (Deng et al., 2017; Amereh et al., 2020). This study found fluorescence-labeled PS-NPs in the seminiferous tubule of the testes and that they negatively affected male reproduction. It suggested that PS-NPs can cross the blood–testis

barrier of mammals, disrupt the meiosis of spermatocytes, and affect spermatogenesis. In the subsequent toxicological experiment, mice were exposed to 50 and 90 nm undecorated PS-NPs orally, mainly because the method of gavage administration in the toxicological test could better simulate the way NPs enter the human body. In contrast, the tail vein injection method could determine the accumulation and distribution of NPs entering the peripheral blood in the organs as efficiently as possible.

Although these recent studies have proved that PS-NPs can accumulate in testicular tissue and cause male reproductive toxicity, including spermatogenesis abnormality and endocrine disturbance, the main effects and mechanisms of spermatogenesis abnormalities caused by PS-NPs are unclear. In this study, our results found that 50 and 90 nm PS-NPs affected testosterone levels, sperm survival, and morphology after 30, 45, and 60 d of exposure, and recent studies have revealed similar results (Amereh et al., 2020; Jin et al., 2021). Furthermore, we found that spermatogenic cells are the target of PS-NPs by detecting pathological characteristics of the testis, specific gene expression of spermatocytes, and the localization of fluorescence-labeled PS-NP particles in testes. Lusher et al. (2017) found that microplastic particles cause the systemic inflammation of fish and then break the integrity of the blood–testis barrier and permeability, thus increasing the chances of plastic particles entering the lumen of the seminiferous tubules. Archibong et al. (2018) suggested that deposited particles cause oxidative stress, increase the extracellular ROS level in the testis, and damage spermatozoa. These studies, including ours, indicate that PS-NPs could easily enter the bloodstream via intestinal absorption and cross the blood–testis barrier, and PS-NP attacks on various types of testicular cells should be investigated further. In this study, mice were gavaged with 50 and 90 nm PS-NPs at doses ranging from 3 to 75 mg/(kg·d) for 30–60 d. Meng et al. (2022) studied the renal toxicity of 50 nm PS-NPs by gavage at doses of 5 mg per mouse for four weeks. In a study by Xu et al. (2021), 50 nm PS-NPs were given to mice by gavage at doses of 5 mg per mouse for 28 d to study the systematic toxicity. In these studies, 50 nm PS-NPs were applied at doses of 5 mg per mouse, calculated based on about 20 g per mouse, which is significantly higher than that of our study. According to the dose conversion and weight between mice and

humans (Nair and Jacob, 2016), in this study, the PS-NP exposure doses to mice were 3–75 mg/kg, which is equivalent to 0.243–6.075 mg/kg to humans (Fu et al., 2023). In terms of exposure concentration in vitro, the results of this study demonstrated that more than 25 µg/mL of 50 nm PS-NPs and more than 75 µg/mL of 90 nm PS-NPs significantly affect the viability of the spermatocyte cell line GC-2. Although no studies have been conducted on the exposure of GC-2 cells to NPs, the concentration of NP treatment used in this study was based on some of the most recent studies. Cortés et al. (2020) found that exposure to more than 200 µg/mL of 50 nm PS-NPs for 24 h could markedly reduce the viability of human intestinal epithelial Caco-2 cells. Xu et al. (2019) found that 25 µg/mL or higher doses of 25 nm PS-NPs and 160 µg/mL or higher doses of 70 nm PS-NPs for 24 h significantly affected the viability and proliferation of human alveolar cell lines A549. Jung et al. (2020) found that the cell function of primary nerve cells was affected by 50 µg/mL of 100 nm PS-NPs for 24 h. Collectively, the exposure doses used in these published studies are similar to ours, and all these results suggest that the particle diameter of PS-NPs is an important factor contributing to its toxic effects on target cells.

This study also found that the differential genes of NPs exposed to GC-2 cells were enriched in ferroptosis and redox pathways by RNA-seq and cluster analyses, and only the inhibitor of ferroptosis (Fer-1) rescues the viability of affected PS-NPs. Fer-1, an ROS-specific ferroptosis inhibitor, has been widely used in ferroptosis research (Dixon et al., 2012). The expression of GPX4 and Nrf2 was then measured, and the results showed that NP exposure decreased GPX4 expression while increasing Nrf2. GPX4 is a lipid repair enzyme that acts as a key regulatory factor in ferroptosis and resists oxygen-dependent lipid peroxidation by converting lipid peroxides (L-OOH) to non-toxic lipids and eliminating phospholipid peroxides (Song and Long, 2020; Stockwell et al., 2020). Nrf2, an essential transcription factor of oxidative responses, maintains cell homeostasis against ferroptosis by regulating the metabolism of glutathione, iron, lipids, and mitochondrial function (Dodson et al., 2019). *GPX4* is one of the Nrf2 target genes and a primary regulator in ferroptosis (Kerins and Ooi, 2018). Conventionally, the expression of GPX4 was positively upregulated by its upstream transcription factor Nrf2; however, in

this study, the expression levels of Nrf2 and GPX4 in PS-NPs-exposed GC-2 cells are the opposite. This may be because PS-NPs induce excessive oxidative stress and cause the depletion of GPX4 and ferroptosis (Imai et al., 2009; Li SB et al., 2021). Generally, Keap1 is a primary regulator of Nrf2; under basal conditions, Nrf2 is bound by Keap1 and forms a complex with Keap1-Cullin3 (CUL3)-ring box protein 1 (RBX1)-E3 ubiquitin ligase, degraded by targeted ubiquitination (Tao et al., 2017). However, under oxidative stress, Nrf2 is released by Keap1 and E3 complex to form dissociated Nrf2, which can promote the nuclear translation involved in several detoxification enzymes and cytoprotective genes into the nucleus (Lu et al., 2021). As a critical regulator of the antioxidant response, Nrf2 has been shown to mitigate lipid peroxidation and ferroptosis by regulating the target genes. These genes include three broad classes—iron/metal metabolism, intermediate metabolism, and GSH synthesis/metabolism, and are verified as antioxidant response elements (AREs) (Dodson et al., 2019). Moreover, our results indicated that the regulatory role of Nrf2 would be affected by PS-NPs based on the results of Nrf2 expression in the nucleus and cytoplasm and the combination of Keap1 with Nrf2. The main characteristics of ferroptosis include mitochondrial shrinkage and cristae reduction, accompanied by increased intracellular Fe^{2+} , ROS, and lipid peroxidation (Tang et al., 2021). Certainly, the characteristics of ferroptosis in PS-NPs-induced GC-2 cells were verified in the present study, and our results indicated that PS-NPs cause ferroptosis in spermatocytes. Subsequently, the results demonstrated that Fer-1 could rescue the PS-NPs-induced ferroptosis at the intracellular Fe^{2+} accumulation, MDA and GSH levels. It has been confirmed that Fer-1 can inhibit ferroptosis by directly inhibiting the production of ROS (Miotto et al., 2020). GSH is a synthetic substrate of GPX4 and is essential for the lipid repair function of GPX4; it is formed from extracellular cystine to intracellular glutamate by the cystine transmembrane cysteine-glutamate antiporter system X_c^- composed of solute carrier family 7 member 11 (SLC7A11) and SLC3A2 (Ursini and Maiorino, 2020; Du et al., 2022). MDA is a major breakdown product of lipid peroxidation reduced to fatty alcohol (LOOH) by GPX4 (Park et al., 2021); in addition, the intracellular Fe^{2+} , MDA, GSH, and lipid peroxidation levels are regarded as ferroptosis biomarkers (Chen et al., 2021), which were also tested in our study.

This study found that PS-NPs affected the expression of iron metabolism-related proteins, including TFR, TF, DMT1, FPN1, HO-1, and the crucial regulators of ferroptosis Nrf2 and GPX4. However, these changed effects were reversed by Fer-1. These results indicated that PS-NPs caused ferroptosis by affecting iron metabolism, which involves important Nrf2-regulated proteins. It is reported that numerous iron-related proteins for metabolism, storage, and transport are regulated by Nrf2 (Lu et al., 2021). The primary function of TF and its receptor TFR is to transport exogenous iron into cells. DMT1 promotes iron into an LIP in the cytoplasm, and FPN1 (SLC40A1) is the only known mammalian protein accounting for iron export from the cells (Liu et al., 2021). The function of HO-1 is to metabolize heme to biliverdin, Fe^{2+} , and carbon monoxide (Kim et al., 2021). The form of LIP is caused by the accumulation of excessive free divalent iron in cells, and it can facilitate the formation of lipid ROS through the Fenton reaction (Liu et al., 2021). According to this study, PS-NPs promote the exogenous Fe^{3+} transport into cells by increasing the expression of TF and TFR and their forming complex. The trapped Fe^{3+} is released in the cytoplasm as the free Fe^{2+} in LIP through DMT1 decreases PS-NPs (Jiang et al., 2021). Additionally, PS-NPs attenuate iron export by decreasing the expression of FPN1. It is reported that TFR, FPN1, HO-1, and other iron homeostasis-related Nrf2-regulated proteins are involved in ferroptosis events (Song and Long, 2020). In fact, as the gatekeeper of Fe^{2+} , FPN1 plays a key role in controlling ferroptosis, not only ensuring the supply of iron for normal function but also avoiding iron overload and inducing oxidative stress (Harada et al., 2011). FPN1 is regulated by the balance of the transcriptional activator Nrf2 and the repressor BACH1 (BRCA-1-associated C-terminal helicase); in the presence of heme, BACH1 inhibits FPN1 transcription and Nrf2 is not able to initiate FPN1 transcription until FPN1 is completely degraded (Riedelberger et al., 2020). Therefore, Nrf2 activation is expected to reduce LIP by upregulating iron storage protein (ferritin) and iron export protein (FPN1) expression. However, in this study, PS-NPs activated Nrf2 and induced the upregulation of iron import proteins TF and TFR and the downregulation of export protein FPN1, resulting in LIP increase and ferroptosis. The results indicated that PS-NPs interfered with the regulation of iron metabolism by Nrf2,

and the decrease of FPN1 expression may be related to its ubiquitin (Jiang et al., 2021), which needs to be further studied. Subsequently, Nrf2 function was inhibited by its specific inhibitor ML385, based on PS-NP exposure. When Nrf2 is unable to enter the nucleus and initiate transcription of those genes, the expression of iron metabolism-related proteins should be reduced. On the contrary, the expression of TFR, DMT1, FPN1, HO-1, and GPX4 was aggravated after Nrf2 restraint when compared to the control and PS-NPs-exposed groups. In addition, this phenotype was further confirmed when siRNA interfered with Nrf2. Therefore, these results suggested that Nrf2 may play a protective role in the process of oxidative stress induced by PS-NPs. However, the antioxidant effect of Nrf2 cannot be offset when it produces stronger oxidative stress, and iron metabolism-related proteins may not be regulated by Nrf2 during ferroptosis. This hypothesis needs to be further studied. Meanwhile, the mechanism by which Nrf2 regulates ferroptosis has been validated in vivo, and the ferroptosis inhibitor Fer-1 alleviated the male reproductive toxicity caused by PS-NPs while the Nrf2 inhibitor aggravated it.

Although this study explored the mechanisms by which PS-NPs cause male reproductive toxicity through inducing ferroptosis in spermatocytes, there are still a few limitations. (1) The dosages of PS-NPs were obtained from the concentration of the toxic effect in the experiment and by referring to the existing literature; however, these dosages do not better simulate the level of exposure in humans due to the lack of epidemiological data on NP exposure. As a result, some toxicological studies on the health risks of NPs to human reproduction may be premature because current exposure levels in humans are much lower than the minimum exposure does in mice. (2) The primary three cell types, including germ cells, Leydig cells, and Sertoli cells, play an important role in spermatogenesis; for example, Leydig cells secrete testosterone and promote spermatogenesis, and Sertoli cells provide nutritional support for germ cells—only these normally functional cell types are required for normal spermatogenesis. In this study, we focused on the effect of PS-NPs on spermatocytes and the induction of reproductive toxicity, and future research should look into how PS-NPs affect spermatogenesis throughout the testis. Furthermore, we believe that research on the transfer efficiency, cumulative time, detection technologies, other adsorbed

pollutants, different diameters and charges of NPs, and the epidemiology of NP exposure should be reinforced, and people must understand the health hazards of NPs to humans.

4 Conclusions

This study uncovered the mechanisms of PS-NPs-triggered male reproductive toxicity through spermatocyte ferroptosis, as summarized in Fig. 7. This study also provided a novel insight into the mechanisms of ferroptosis induced by PS-NPs, which involve the key role of Nrf2 in regulating iron metabolism and redox homeostasis. On the one hand, Nrf2 activation enhances Fe^{3+} import, reduces Fe^{2+} export, and results in LIP accumulation; on the other hand, PS-NPs disturb

the progress of Nrf2, regulate antioxidation, and accelerate ferroptosis. The antioxidation produced by Nrf2 and activated by PS-NPs cannot eliminate the LIP accumulation caused by Nrf2-enhanced iron metabolism, which then induces ferroptosis by increasing the Fenton reaction. Meanwhile, this study also implied a therapeutic strategy for male reproductive diseases by enhancing free iron excretion and oxidative stress clearance capacity by targeting Nrf2.

Materials and methods

Detailed methods are provided in the electronic supplementary materials of this paper.

Data availability statement

All datasets analyzed in this study are available from the corresponding author upon request.

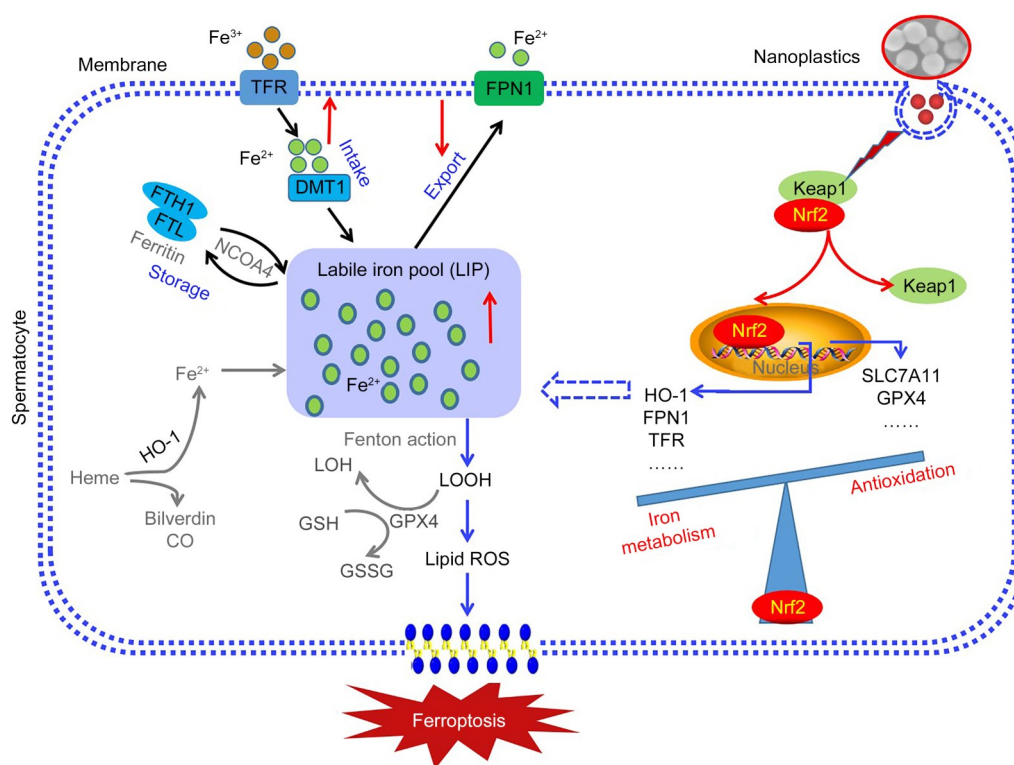


Fig. 7 Schematic of Nrf2-mediated PS-NPs-induced ferroptosis-related mechanisms in spermatocytes. PS-NPs induced spermatocyte ferroptosis through iron homeostasis imbalance and antioxidation decrease dependent on Nrf2. Mechanistically, as a key regulator of the antioxidant response and iron metabolism, Nrf2 is activated by PS-NPs by releasing from Keap1 and entering the nucleus in the spermatocyte. Meanwhile, Nrf2 protects cells from PS-NPs-triggered ferroptosis by regulating iron metabolism and lipid redox homeostasis-related proteins. On the one hand, Nrf2 activation enhances Fe^{3+} import, reduces Fe^{2+} export, and results in LIP accumulation; on the other hand, PS-NPs disturb Nrf2 progression, regulate GPX4 expression, and accelerate ferroptosis. Nrf2: nuclear factor erythroid 2-related factor 2; PS-NPs: polystyrene nanoparticles; Keap1: Kelch-like ECH-associated protein 1; GPX4: glutathione peroxidase 4; TFR: transferrin receptor; FPN1: ferroportin 1; DMT1: divalent metal transporter 1; FTH1: ferritin heavy chain 1; FTL: ferritin light polypeptide; NCOA4: nuclear receptor coactivator 4; HO-1: hemoxygenase-1; LOH: lipid alcohol; LOOH: lipid hydrogen peroxide; ROS: reactive oxygen species; GSH: glutathione; GSSG: glutathione disulfide; SLC7A11: solute carrier family 7 member 11.

Acknowledgments

This work was supported by the National Natural Science Foundation of China (No. 82204094), the Key Research and Development Program of Ningxia (No. 2022BEG03084), and the National Key Research and Development Program of China (No. 2018YFC1004202).

Author contributions

Hang HAN, Hong YANG, Bo XU, Wenjie DAI, Ling LIU, and Tiantian HE performed the experimental research and data analysis. Xufeng FU and Xiuying PEI wrote and edited the manuscript. Xufeng FU and Xing DU contributed to the study design, data analysis, writing and editing of the manuscript. All authors have read and approved the final manuscript, and therefore, have full access to all the data in the study and take responsibility for the integrity and security of the data.

Compliance with ethics guidelines

Xufeng FU, Hang HAN, Hong YANG, Bo XU, Wenjie DAI, Ling LIU, Tiantian HE, Xing DU, and Xiuying PEI declare that they have no conflict of interest.

The animal experiments were carried out under the approval of the Institutional Animal Care and Use Committee of Ningxia Medical University (No. NXMU-2022-G073).

References

- Amerah F, Babaei M, Eslami A, et al., 2020. The emerging risk of exposure to nano(micro)plastics on endocrine disturbance and reproductive toxicity: from a hypothetical scenario to a global public health challenge. *Environ Pollut*, 261:114158. <https://doi.org/10.1016/j.envpol.2020.114158>
- Archibong AE, Rideout ML, Harris KJ, et al., 2018. Oxidative stress in reproductive toxicology. *Curr Opin Toxicol*, 7:95-101. <https://doi.org/10.1016/j.cotox.2017.10.004>
- Bisht S, Faiq M, Tolahunase M, et al., 2017. Oxidative stress and male infertility. *Nat Rev Urol*, 14(8):470-485. <https://doi.org/10.1038/nrurol.2017.69>
- Chen X, Comish PB, Tang DL, et al., 2021. Characteristics and biomarkers of ferroptosis. *Front Cell Dev Biol*, 9:637162. <https://doi.org/10.3389/fcell.2021.637162>
- Cortés C, Domenech J, Salazar M, et al., 2020. Nanoplastics as a potential environmental health factor: effects of polystyrene nanoparticles on human intestinal epithelial Caco-2 cells. *Environ Sci Nano*, 7(1):272-285. <https://doi.org/10.1039/C9EN00523D>
- Deng YF, Zhang Y, Lemos B, et al., 2017. Tissue accumulation of microplastics in mice and biomarker responses suggest widespread health risks of exposure. *Sci Rep*, 7:46687. <https://doi.org/10.1038/srep46687>
- Dixon SJ, Lemberg KM, Lamprecht MR, et al., 2012. Ferroptosis: an iron-dependent form of nonapoptotic cell death. *Cell*, 149(5):1060-1072. <https://doi.org/10.1016/j.cell.2012.03.042>
- Dodson M, Castro-Portuguez R, Zhang DD, 2019. NRF2 plays a critical role in mitigating lipid peroxidation and ferroptosis. *Redox Biol*, 23:101107. <https://doi.org/10.1016/j.redox.2019.101107>
- Du FN, Cai HW, Zhang Q, et al., 2020. Microplastics in take-out food containers. *J Hazard Mater*, 399:122969. <https://doi.org/10.1016/j.jhazmat.2020.122969>
- Du X, Zhang JJ, Liu L, et al., 2022. A novel anticancer property of *Lycium barbarum* polysaccharide in triggering ferroptosis of breast cancer cells. *J Zhejiang Univ-Sci B (Biomed & Biotechnol)*, 23(4):286-299. <https://doi.org/10.1631/jzus.B2100748>
- Fendall LS, Sewell MA, 2009. Contributing to marine pollution by washing your face: microplastics in facial cleansers. *Mar Pollut Bull*, 58(8):1225-1228. <https://doi.org/10.1016/j.marpolbul.2009.04.025>
- Fu XF, Liu L, Han H, et al., 2023. Integrated fecal microbiome and metabolome analysis explore the link between polystyrene nanoplastics exposure and male reproductive toxicity in mice. *Environ Toxicol*, 38(6):1277-1291. <https://doi.org/10.1002/tox.23763>
- Gasperi J, Wright SL, Dris R, et al., 2018. Microplastics in air: are we breathing it in? *Curr Opin Environ Sci Health*, 1:1-5. <https://doi.org/10.1016/j.coesh.2017.10.002>
- Harada N, Kanayama M, Maruyama A, et al., 2011. Nrf2 regulates ferroportin 1-mediated iron efflux and counteracts lipopolysaccharide-induced ferroportin 1 mRNA suppression in macrophages. *Arch Biochem Biophys*, 508(1):101-109. <https://doi.org/10.1016/j.abb.2011.02.001>
- Hassannia B, Vandenabeele P, Berghe TV, 2019. Targeting ferroptosis to iron out cancer. *Cancer Cell*, 35(6):830-849. <https://doi.org/10.1016/j.ccell.2019.04.002>
- Hernandez LM, Xu EG, Larsson HCE, et al., 2019. Plastic teabags release billions of microparticles and nanoparticles into tea. *Environ Sci Technol*, 53(21):12300-12310. <https://doi.org/10.1021/acs.est.9b02540>
- Huang C, Li BS, Xu KR, et al., 2017. Decline in semen quality among 30,636 young Chinese men from 2001 to 2015. *Fertil Steril*, 107(1):83-88.e2. <https://doi.org/10.1016/j.fertnstert.2016.09.035>
- Imai H, Hakkaku N, Iwamoto R, et al., 2009. Depletion of selenoprotein GPx4 in spermatocytes causes male infertility in mice. *J Biol Chem*, 284(47):32522-32532. <https://doi.org/10.1074/jbc.M109.016139>
- Jiang L, Wang JM, Wang K, et al., 2021. RNF217 regulates iron homeostasis through its E3 ubiquitin ligase activity by modulating ferroportin degradation. *Blood*, 138(8):689-705. <https://doi.org/10.1182/blood.2020008986>
- Jin HB, Ma T, Sha XX, et al., 2021. Polystyrene microplastics induced male reproductive toxicity in mice. *J Hazard Mater*, 401:123430. <https://doi.org/10.1016/j.jhazmat.2020.123430>
- Jung BK, Han SW, Park SH, et al., 2020. Neurotoxic potential of polystyrene nanoplastics in primary cells originating from mouse brain. *Neurotoxicology*, 81:189-196. <https://doi.org/10.1016/j.neuro.2020.10.008>

- Kedzierski M, Lechat B, Sire O, et al., 2020. Microplastic contamination of packaged meat: occurrence and associated risks. *Food Packag Shelf Life*, 24:100489. <https://doi.org/10.1016/j.fpsl.2020.100489>
- Kerins MJ, Ooi A, 2018. The roles of NRF2 in modulating cellular iron homeostasis. *Antioxid Redox Signal*, 29(17):1756-1773. <https://doi.org/10.1089/ars.2017.7176>
- Khan FR, Catarino AI, Clark NJ, 2022. The ecotoxicological consequences of microplastics and co-contaminants in aquatic organisms: a mini-review. *Emerg Top Life Sci*, 6(4):339-348. <https://doi.org/10.1042/ETLS20220014>
- Kim MJ, Yun GJ, Kim SE, 2021. Metabolic regulation of ferroptosis in cancer. *Biology*, 10(2):83. <https://doi.org/10.3390/biology10020083>
- Levine H, Jørgensen N, Martino-Andrade A, et al., 2017. Temporal trends in sperm count: a systematic review and meta-regression analysis. *Hum Reprod Update*, 23(6):646-659. <https://doi.org/10.1093/humupd/dmx022>
- Li SB, He YP, Chen KX, et al., 2021. RSL3 drives ferroptosis through NF-κB pathway activation and GPX4 depletion in glioblastoma. *Oxid Med Cell Longev*, 2021:2915019. <https://doi.org/10.1155/2021/2915019>
- Li YM, Liu ZQ, Yang Y, et al., 2021. Effects of nanoplastics on energy metabolism in the oriental river prawn (*Macrobrachium nipponense*). *Environ Pollut*, 268:115890. <https://doi.org/10.1016/j.envpol.2020.115890>
- Liu ZX, Lv XY, Yang BW, et al., 2021. Tetrachlorobenzoquinone exposure triggers ferroptosis contributing to its neurotoxicity. *Chemosphere*, 264:128413. <https://doi.org/10.1016/j.chemosphere.2020.128413>
- Lu J, Zhao YN, Liu MT, et al., 2021. Toward improved human health: Nrf2 plays a critical role in regulating ferroptosis. *Food Funct*, 12(20):9583-9606. <https://doi.org/10.1039/d1fo01036k>
- Lusher A, Hollman P, Mendoza-Hill J, 2017. Microplastics in Fisheries and Aquaculture: Status of Knowledge on Their Occurrence and Implications for Aquatic Organisms and Food Safety. FAO Fisheries and Aquaculture Technical Paper No. 615, Food and Agriculture Organization of the United Nations, Madrid.
- Meng XM, Zhang JW, Wang WJ, et al., 2022. Effects of nano- and microplastics on kidney: physicochemical properties, bioaccumulation, oxidative stress and immunoreaction. *Chemosphere*, 288(Pt 3):132631. <https://doi.org/10.1016/j.chemosphere.2021.132631>
- Miotto G, Rossetto M, di Paolo ML, et al., 2020. Insight into the mechanism of ferroptosis inhibition by ferrostatin-1. *Redox Biol*, 28:101328. <https://doi.org/10.1016/j.redox.2019.101328>
- Nair AB, Jacob S, 2016. A simple practice guide for dose conversion between animals and human. *J Basic Clin Pharm*, 7(2):27-31. <https://doi.org/10.4103/0976-0105.177703>
- Oßmann BE, Sarau G, Holtmannspötter H, et al., 2018. Small-sized microplastics and pigmented particles in bottled mineral water. *Water Res*, 141:307-316. <https://doi.org/10.1016/j.watres.2018.05.027>
- Park MW, Cha HW, Kim J, et al., 2021. NOX4 promotes ferroptosis of astrocytes by oxidative stress-induced lipid peroxidation via the impairment of mitochondrial metabolism in Alzheimer's diseases. *Redox Biol*, 41:101947. <https://doi.org/10.1016/j.redox.2021.101947>
- Ragusa A, Svelato A, Santacroce C, et al., 2021. Plasticenta: first evidence of microplastics in human placenta. *Environ Int*, 146:106274. <https://doi.org/10.1016/j.envint.2020.106274>
- Riedelberger M, Penninger P, Tscherner M, et al., 2020. Type I interferon response dysregulates host iron homeostasis and enhances *Candida glabrata* infection. *Cell Host Microbe*, 27(3):454-466.e8. <https://doi.org/10.1016/j.chom.2020.01.023>
- Rist S, Baun A, Hartmann NB, 2017. Ingestion of micro- and nanoplastics in *Daphnia magna* – quantification of body burdens and assessment of feeding rates and reproduction. *Environ Pollut*, 228:398-407. <https://doi.org/10.1016/j.envpol.2017.05.048>
- Schulte RT, Ohl DA, Sigman M, et al., 2010. Sperm DNA damage in male infertility: etiologies, assays, and outcomes. *J Assist Reprod Genet*, 27(1):3-12. <https://doi.org/10.1007/s10815-009-9359-x>
- Shukla S, Khan R, Saxena A, et al., 2022. Microplastics from face masks: a potential hazard post Covid-19 pandemic. *Chemosphere*, 302:134805. <https://doi.org/10.1016/j.chemosphere.2022.134805>
- Song XH, Long DX, 2020. Nrf2 and ferroptosis: a new research direction for neurodegenerative diseases. *Front Neurosci*, 14:267. <https://doi.org/10.3389/fnins.2020.00267>
- Stockwell BR, Jiang XJ, Gu W, 2020. Emerging mechanisms and disease relevance of ferroptosis. *Trends Cell Biol*, 30(6):478-490. <https://doi.org/10.1016/j.tcb.2020.02.009>
- Sun XF, Ou ZH, Chen RC, et al., 2016. Activation of the p62-Keap1-NRF2 pathway protects against ferroptosis in hepatocellular carcinoma cells. *Hepatology*, 63(1):173-184. <https://doi.org/10.1002/hep.28251>
- Tang DL, Chen X, Kang R, et al., 2021. Ferroptosis: molecular mechanisms and health implications. *Cell Res*, 31(2):107-125. <https://doi.org/10.1038/s41422-020-00441-1>
- Tao SS, Liu PF, Luo G, et al., 2017. p97 negatively regulates NRF2 by extracting ubiquitylated NRF2 from the KEAP1-CUL3 E3 complex. *Mol Cell Biol*, 37(8):e00660-16. <https://doi.org/10.1128/MCB.00660-16>
- Ursini F, Maiorino M, 2020. Lipid peroxidation and ferroptosis: the role of GSH and GPx4. *Free Radic Biol Med*, 152:175-185. <https://doi.org/10.1016/j.freeradbiomed.2020.02.027>
- Wang LW, Wu WM, Bolan NS, et al., 2021. Environmental fate, toxicity and risk management strategies of nanoplastics in the environment: current status and future perspectives. *J Hazard Mater*, 401:123415. <https://doi.org/10.1016/j.jhazmat.2020.123415>
- Wang Z, An CJ, Chen XJ, et al., 2021. Disposable masks release

- microplastics to the aqueous environment with exacerbation by natural weathering. *J Hazard Mater*, 417:126036. <https://doi.org/10.1016/j.jhazmat.2021.126036>
- Xu DH, Ma YH, Han XD, et al., 2021. Systematic toxicity evaluation of polystyrene nanoplastics on mice and molecular mechanism investigation about their internalization into Caco-2 cells. *J Hazard Mater*, 417:126092. <https://doi.org/10.1016/j.jhazmat.2021.126092>
- Xu MK, Halimu G, Zhang QR, et al., 2019. Internalization and toxicity: a preliminary study of effects of nanoplastic particles on human lung epithelial cell. *Sci Total Environ*, 694:133794. <https://doi.org/10.1016/j.scitotenv.2019.133794>
- Yee MSL, Hii LW, Looi CK, et al., 2021. Impact of microplastics and nanoplastics on human health. *Nanomaterials*, 11(2):496. <https://doi.org/10.3390/nano11020496>
- Yin K, Wang Y, Zhao HJ, et al., 2021. A comparative review of microplastics and nanoplastics: toxicity hazards on digestive, reproductive and nervous system. *Sci Total Environ*, 774:145758. <https://doi.org/10.1016/j.scitotenv.2021.145758>
- Yin LS, Wen XF, Huang DL, et al., 2021. Interactions between microplastics/nanoplastics and vascular plants. *Environ Pollut*, 290:117999. <https://doi.org/10.1016/j.envpol.2021.117999>
- Yong CQY, Valiyaveetil S, Tang BL, 2020. Toxicity of microplastics and nanoplastics in mammalian systems. *Int J Environ Res Public Health*, 17(5):1509. <https://doi.org/10.3390/ijerph17051509>
- Yosri N, Khalifa SAM, Guo ZM, et al., 2021. Marine organisms: pioneer natural sources of polysaccharides/proteins for green synthesis of nanoparticles and their potential applications. *Int J Biol Macromol*, 193:1767-1798. <https://doi.org/10.1016/j.ijbiomac.2021.10.229>
- Zegers-Hochschild F, Adamson GD, Dyer S, et al, 2017. The international glossary on infertility and fertility care, 2017. *Fertil Steril*, 108(3):393-406. <https://doi.org/10.1016/j.fertnstert.2017.06.005>

Supplementary information

Materials and methods; Figs. S1–S6